JOURNAL OF SPACECRAFT AND ROCKETS
Vol. 33, No. 1, January–February 1996

Local Effects of Solid Rocket Motor Exhaust on Stratospheric Ozone

Martin Ross*
The Aerospace Corporation, Los Angeles, California 90009

Solid rocket motor (SRM) exhaust contains chlorine, an important stratospheric constituent that plays a crucial role in the chemistry of ozone. Models of SRM plume combustion and chemistry suggest that a significant fraction of SRM exhaust chlorine might be in an active form as a result of afterburning reactions and be available for immediate ozone destruction as the plume mixes with the ambient stratosphere. If afterburning does produce free chlorine, the SRMs used by the Titan IV and Space Shuttle have the potential to cause nearly complete ozone loss in regions up to several tens of kilometers in radius, depending on altitude. We present a simulation of SRM exhaust mixing and chemistry that predicts the three-dimensional structure of the prompt local ozone loss during the 8 h following a daytime Titan IV launch. Maps of the loss of the total column ozone abundance show that the maximum loss of about 30% occurs about one hour after launch. Four hours after launch the area of column ozone loss exceeding 8% covers up to 2000 km^2. The shape and severity of the ozone-depleted region depends only slightly on the interaction between launch trajectory and stratospheric winds. Solar ultraviolet flux on the ground beneath the plume changes in response to decreased ozone absorption, alumina scattering, and absorption by chlorine oxide compounds. The ultraviolet flux increases by 100% at 295 nm, shows no change near 300 nm, and decreases by 30% longward of 310 nm. Existing space instrumentation does not possess the spatial resolution required to measure ozone depletion of the size and magnitude predicted following launches involving large SRMs.

Nomenclature

a = aerosol particle radius
D = turbulent diffusion coefficient
I_s = solar radiance at the top of the atmosphere
I_t = solar radiance at the top of the troposphere
N = aerosol size distribution
n_i = number density of ith species
Q = aerosol scattering efficiency
r = radial distance from solid rocket motor plume center
u = zonal wind velocity
v = meridional wind velocity
z = altitude
Γ_i = total column abundance of ith species
λ = wavelength
σ_i = absorption cross section of ith species
τ_a = absorbing optical depth of stratospheric species
τ_s = scattering optical depth of plume alumina
Ω = total column abundance of ozone

Introduction

SOLID-FUEL rocket motors (SRMs) that use ammonium perchlorate oxidizer deposit chlorine compounds directly into the stratosphere up to about 40-km altitude. Chlorine plays a pivotal role in stratospheric chemistry and is one of the main determinants of ozone concentrations in the stratosphere. Sudden injection of atomic or molecular chlorine into the stratosphere will cause a prompt, local depletion of ozone that will persist until ozone-rich air is mixed into the depleted region by stratospheric diffusion. Space Shuttle and Titan IV SRM exhaust deposits several tons of chlorine per kilometer of altitude, and if a significant fraction of the chlorine is in an active form, the local ozone depletion will encompass tens to hundreds of square kilometers, depending on altitude, and last for several hours. SRM use also has global implications for stratospheric chemistry that do not depend on whether the exhaust chlorine is active or not. The conclusion in this regard is that current levels of SRM use cause a small amount of steady-state global ozone depletion, a fraction of a percent loss of the total ozone column abundance.[1–3] In this work we limit our attention to the local effects of SRM exhaust during the first day after launch, when exhaust compounds dominate the chemistry in the expanding plume and the ozone column might be depleted by tens of percent or more.

We begin by assuming that a significant fraction of the chlorine in the plume ultimately appears as Cl or Cl_2. Most of the chlorine in the exhaust is contained in HCl as it leaves the motor nozzle. The composition of the exhaust as it begins to mix with the stratosphere will be different from the composition at the motor nozzle, however. Afterburning reactions are known to occur in the hot plume hundreds of meters downstream from the motor nozzle. The main afterburning reactions produce CO_2 and H_2O from CO, H_2, and ambient O_2 entrained in the plume. Recently, several investigators, using a widely accepted model of SRM hot-plume chemistry and mixing, have concluded that HCl will react with H, OH, and O in the afterburning region to produce free chlorine.[4,5] The model predicts that 30–80% of exhaust chlorine will be in the form Cl or Cl_2, the fraction increasing with altitude. These predictions form the basis for the cold-plume model presented here. It must be acknowledged that afterburning of HCl in SRM plumes has not been proven to occur. Our results are model-dependent in this regard. If afterburning does not produce significant fractions of free chlorine, the local effects on ozone will be muted compared to the results presented here. There is at present little data to confirm or deny the production of free chlorine in the hot plume. One investigation aboard a 1973 sampling flight through a Titan III SRM plume at 18-km altitude found 40% ozone loss,[6] an amount most easily understood as providing evidence of significant HCl afterburning.

Previous models of the prompt local effects of SRM exhaust on stratospheric chemistry do not entirely agree on the basic features of the magnitude and timescale of ozone loss. Karol et al.[7] used a 98-reaction stratospheric chemistry scheme and considered scenarios with different amounts of free-chlorine production in the Space Shuttle SRMs. For the case with substantial active chlorine production they predict nearly 100% ozone loss at all affected levels over regions several kilometers in radius for several hours after launch. Denison et al.[5] presented a detailed and realistic SRM exhaust chemistry scheme including afterburning. For the case of a relatively small motor, about $\frac{1}{10}$ the mass of the Titan IV motors, they found nearly complete ozone loss over a region about 1 km in diameter lasting

Received Nov. 30, 1994; revision received Aug. 20, 1995; accepted for publication Aug. 28, 1995.

*Member Technical Staff, Space and Environment Technology Center, P.O. Box 92957.

several hundred seconds. Kruger[8] modeled the local effects of the Space Shuttle using different assumptions of free-chlorine production and found significant ozone loss over regions up to 10 km from the plume center up to an hour after launch. Different assumptions regarding vehicle type, afterburning, and liquid-motor hot-plume chemistry likely account for the different results among these investigations, but together they strongly suggest the possibility of significant prompt local ozone loss because of SRM exhaust.

Each of these efforts failed to consider the three-dimensional transport and mixing behavior of the plume and the vertically integrated ozone loss in the expanding plume. The shape, intensity, and location of the disturbed region is determined by the interplay between the stratospheric winds, the direction of the launch, and the diffusion and chemistry of the plume. The location and magnitude of the total column abundance of important plume species, including ozone, can only be understood within the context of a three-dimensional model of the plume. Total column abundances of absorbing species and scattering aerosols in turn determine the radiative environment in and beneath the plume. Ultimately, the local environmental impact of SRM exhaust ozone depletion depends on the magnitude of the increase in solar ultraviolet radiation reaching the ground under the advecting and shearing plume. This can be evaluated only by including stratospheric wind advection in the description of transport. Finally, in situ and remote measurements of SRM effects on stratospheric chemistry are being considered by various agencies; predictions of plume composition, location, and size are required to effectively plan launch ozone-loss measurement programs.

In this paper we present results from a model of rocket-exhaust stratospheric mixing and chemistry that predicts the diffusion and wind-driven evolution of the cold plume in a three-dimensional sense. The vehicle considered is the Titan IV. The model chemistry includes only the most important reactions involving chlorine and oxygen, a scheme that produces results compatible with the results of models with more complete chemistry. Diffusion and mixing are limited to linear horizontal diffusion with time-dependent diffusion coefficient and two-dimensional wind advection of stratospheric layers. Our model demonstrates the intensity and spatial extent of the local ozone depletion and how the depleted region evolves during the first day after launch. We discuss the eventual demise of the ozone hole as the exhaust compounds become indistinguishable from the ambient stratosphere. We also present a simple model of plume ultraviolet transmittance and predict the perturbation in the ultraviolet flux on the ground beneath the plume. Finally, we point out instrument resolution and sensitivity requirements to measure SRM ozone loss.

Model Description

We consider the evolution of minor species and aerosol number densities in a three-dimensional mesoscale region of the stratosphere given an initial distribution and an appropriate description of stratospheric transport, mixing, and photochemistry. By identifying the species and reactions that are most important to the first-order chemistry in the expanding plume, the numerical demands of the kinetic modeling are eased. We further simplify the model by limiting diffusion to the radial direction and so are able to construct a model that requires only modest integration time. The three-dimensional representation of the expanding plume is done by combining independent solutions from different altitudes in a way that mimics large-scale transport. The details of these simplifications are discussed in the following sections.

For a minor species in a turbulent fluid with constant background flow, the rate of change of minor species concentration n_i can be written

$$\dot{n}_i = T[n_i(x)] + (P_i - L_i) \qquad (1)$$

where T is an operator on the spatial distribution of n_i, and P_i and L_i are the total chemical production and loss terms, respectively. The operator T represents dynamic effects over all length scales, which in general include material diffusion and advection in the background flow. We note that the two timescales implied by the right-hand side of Eq. (1), dynamical and chemical, are comparable for several important plume components. In this paper, we discuss the model chemistry used to calculate the rates P_i and L_i and present arguments proposing that the effects of small-scale turbulence and the large-scale background flow in the stratosphere are separable, so that a simple form for T can be used in Eq. (1).

Equation (1) was solved using an implicit finite difference time-stepping scheme[9] with 60 radial grid points, spacing of 0.5 km, and variable time step. Calculations were carried out for 25 levels in the stratosphere from the tropopause (assumed 15-km altitude) to the approximate SRM burnout altitude, 40 km. The actual tropopause height and SRM burnout altitude are variable by several kilometers. At both the inner and outer boundaries, the number-density gradients are set to zero.

Photochemical Model

Table 1 lists the reactions in the model oxygen–chlorine atmosphere. Rate constants used are from DeMore et al.[10] This set consists of reactions that are important over the timescale of the local SRM exhaust problem, about 10^4 s. Hydrogen and nitrogen free-radical chemical cycles, important in the unperturbed stratosphere, can be omitted in this model for two reasons. First, these compounds account for only a few percent of SRM exhaust[5] (the Titan IV liquid stages do not burn in the stratosphere). Second, the number density of chlorine compounds from the exhaust greatly exceeds the number density of other minor species in the stratosphere over a large area. This means that chlorine and oxygen reactions dominate the kinetics, and a chemistry scheme based on an oxygen–chlorine atmosphere is a good approximation. For example, $ClONO_2$, an important reservoir species formed by the reaction $ClO + NO_2 + M \rightarrow ClONO_2 + M$, plays only a small part in the expanding plume region as long as the plume is less than about 40 km in radius; other important radicals (OH, NO_2, NO) are overwhelmed to an even greater degree by plume chlorine. The model does include the most important stratospheric chlorine sink for the time and spatial scales of this problem: HCl, formed by reaction of ozone with methane. HCl does not react further with any abundant plume species. We do not consider non-gas-phase reactions, which may take place on SRM exhaust particulate surfaces.[11]

Vertical profiles of photodissociation coefficients are for overhead sun conditions in the undisturbed stratosphere.[12] We do not allow for changes in the radiative environment caused by changes in atmospheric transmission in the extended plume, which might affect photodissociation rates. Rigorously, model composition should feed back into the chemistry through the photodissociation coefficients after the model radiative environment is calculated. This would include absorption and scattering by exhaust species and aerosols, respectively. During the first few minutes of plume evolution, aerosol scattering controls the radiative environment, lessening the intensity of solar radiation in the plume. Later, ozone loss dominates, causing an increase in solar ultraviolet penetration and an increase in photodissociation rates at some altitudes. The main effect would be to change the photodissociation rates of Cl_2 and ClO; the lower stratosphere would be more affected than the upper in this

Table 1 Reactions in the kinetics scheme

$O_2 + h\nu \rightarrow 2O$
$O_3 + h\nu \rightarrow O + O_2$
$O + O_2 + M \rightarrow O_3 + M$
$O + O_3 \rightarrow 2O_2$
$O + O + M \rightarrow O_2 + M$
$ClO + h\nu \rightarrow Cl + O$
$ClO + ClO + M \rightarrow Cl_2O_2 + M$
$Cl + O_3 \rightarrow ClO + O_2$
$Cl_2O_2 + h\nu \rightarrow Cl + ClOO$
$ClOO + M \rightarrow Cl + O_2 + M$
$Cl + CH_4 \rightarrow HCl + CH_3$
$HCl + h\nu \rightarrow H + Cl$
$Cl_2 + h\nu \rightarrow 2Cl$
$Cl + Cl_2O_2 \rightarrow Cl_2 + ClOO$
$ClO + O \rightarrow Cl + O_2$

regard. An increase in either rate would increase ozone depletion by freeing additional Cl. The assumption of constant overhead sun ignores the dependence of photodissociation on solar zenith angle χ through time of year, latitude, and local time. However, photodissociation of Cl_2, the most important rate for the cold-plume chemistry, varies with χ by only a few percent throughout the stratosphere for χ less than 60 deg. The photodissociation rates of ClO and Cl_2O_2 will not vary by more than a factor of about 2 for χ less than 60 deg.

We assume the temperature in the plume is constant and equal to the ambient temperature. The plume temperature initially exceeds the ambient stratospheric temperature and cools by diffusive mixing and by rising adiabatically several kilometers during the first 6–12 min after launch. (This behavior is observed in tracking data of SRM plumes in the lower stratosphere.) During the first few minutes after vehicle passage, as the plume is cooling, the rate of change in species concentration in Eq. (1) is dominated by large composition gradients and rapidly varying number densities in the mixing region rather than the chemical production and loss terms, so that ignoring the temperature sensitivity of the reaction rates does not cause significant error.

Stratospheric Transport

By transport we mean the turbulent diffusion of minor species down local number-density gradients and the horizontal advection of stratospheric layers with respect to each other by the stratospheric winds. There is in fact no physical difference between diffusion and advection; both are manifestations of stratospheric motions. A distinction between the two must inevitably be made, however, based on the model grid spacing. The difficulty is that we need to include the dissipative effects of turbulence over subkilometer scales while shearing the plume in the large-scale stratospheric flow over scales of hundreds of kilometers in a numerically tenable model. The dominance of horizontal sub-grid-scale turbulent diffusion over vertical diffusion and the dominance of horizontal large-scale flow over vertical flow allows us to decouple the effects of these motions in the stratosphere and simplify the operator T in Eq. (1).

Turbulent motion in the stratosphere is driven by gradients in the large-scale flow. The turbulent motion in turn causes diffusion down gradients of minor species concentrations at a rate proportional to the magnitude of the gradient.[13] The turbulent motion is isotropic up to scales of about 100 m; at larger scales the eddies become flattened as the thermal stratification discriminates between horizontal and vertical motions.[14] Horizontal diffusion exceeds vertical by several orders of magnitude over the length and time scales of interest here,[14,15] and we can therefore ignore vertical diffusion. Because the diffusion can be assumed isotropic in horizontal layers[14] and the plume is assumed radially symmetric, we describe plume diffusion in cylindrical coordinates.

Strictly, the operator T includes a diffusionlike term proportional to the horizontal gradient of the horizontal winds. This contribution to mixing will be comparable to the turbulent diffusion for wind gradients of a few tens of percent over a few hundred kilometers, a condition that likely obtains in the stratosphere. We ignore this term and assume the background wind is constant in horizontal layers, while noting the potential for horizontal wind gradients to influence plume mixing.

Taken together, these simplifications allows us specify the operator T as

$$T[n_i(x)] = D\nabla_r^2 n_i \tag{2}$$

where ∇_r^2 is the cylindrical Laplacian and the eddy diffusion coefficient D includes all of the diffusive effects of the turbulent flow. The choice of D cannot be made unambiguously. The turbulent diffusion is nonlinear in the sense that the amplitude of the turbulent velocity fluctuations increases with scale length, so that the effective diffusion coefficient increases with scale length. So that the problem will remain linear, the effects of the turbulent-motion nonlinearity are included in a qualitative way by specifying that D increases with time. This type of parametrization has been previously used in stratospheric plume models.[5–7,16] Based on representative values for stratospheric turbulent diffusion coefficients as functions of time and dispersion distance,[15] we find that

$$D = 10^{-2}t^{1.3} \tag{3}$$

(assumed independent of altitude) where D is in $m^2 \cdot s^{-1}$ and t is in seconds. Turbulence frequently appears in patches and layers that can become isolated from the rest of the flow and not participate in the mixing for a period of time. The simple diffusion model remains acceptable for this problem because the most important reactions are fast compared to any plausible mixing rate and there are no chlorine sinks in the SRM exhaust. Were some plume region to stop diffusing and become isolated from the rest of the stratosphere, Cl_2 photolysis would proceed and any unreacted chlorine would wait until the isolated region eventually mixed with ambient air, causing ozone loss. The sequence of reactions is not greatly altered by the existence of isolated patches, only the time and distance scales of the inevitable result.

After integrating Eqs. (1) and (2) for each altitude independently, the solution at a given altitude is given as a function of time and radius from the plume center by $n(r, t)$. The three-dimensional structure of the plume is recovered by translating (i.e., advecting) the plume center (i.e., the origin of the solution) at each altitude from its original position according to a model of zonal and meridional stratospheric wind profiles. The center of the radially diffusing plume at the ith level in a geographic coordinate system $(x_c, y_c)_i$ is given as a function of time by $(x_c, y_c)_i = (x_{c0} + u_i t, y_{c0} + v_i t)$, where the subscript 0 refers to the initial location of the plume, and $u_i(z)$ and $v_i(z)$ are the zonal and meridional winds at the ith level, respectively. This amounts to shifting the horizontal position of each 1-km-thick layer to generate a three-dimensional description of the plume; the scheme is purely kinematic, since there is no relationship between the relative motion of the layers, the vertical shear, and the local rate of turbulent dissipation.

Al_2O_3 Aerosol

Titan IV SRM exhaust contains 28.8% by mass of Al_2O_3 particulates. This exhaust component is important in the context of local effects for reasons involving ozone destruction rates and remote measurements using ultraviolet light. Other possible SRM exhaust aerosols, ice and soot, are likely less important than Al_2O_3 and so are not considered here.[11,17] The severe south polar springtime ozone depletion and the midlatitude ozone loss after large volcanic eruptions demonstrate the efficacy of aerosols in influencing ozone chemistry through heterogeneous reactions.[18] The kinetic characteristics and total surface area of Al_2O_3 particles may be sufficient to influence the local plume chemistry; the relevant kinetic parameters have not been measured, however, and the matter is unresolved.

Al_2O_3 particles scatter light out of the plume, lessening the radiant intensity in and beneath the plume. Scattering can be a serious complication to modeling efforts through the effects on photodissociation rates, discussed above. Scattering also greatly complicates the interpretation of remote-sensing data.[19] For example, an increase in the solar midultraviolet Rayleigh backscatter to space can be interpreted as a decrease in the ozone column abundance or as an increase in the aerosol number density in the column. Multispectral and polarization techniques can, in principle, be applied to separate the aerosol scattering intensity from the Rayleigh scattering intensity, but the analysis effort and instrumentation complexity increase substantially. The Al_2O_2 particles also complicate in situ measurements of plume composition by scattering light from diagnostic light sources and interfering with instrument mechanical operations. Given the influence that SRM aerosols might have on photochemistry and measurements, it is of interest to calculate the Al_2O_2 number density in the plume under the assumption that alumina particles diffuse in the manner of the exhaust gases.

The size distribution of the exhaust alumina is not well understood. No particular size distribution is widely accepted as valid for SRM combustion in the stratosphere over all particle sizes. We adopt the distribution reported by Cofer et al.[20] based on several measurements of Space Shuttle exhaust at different tropospheric altitudes:

$$N(a) = \alpha\, 10^{-1.78a} \tag{4}$$

where the units of N are $cm^{-3} \cdot \mu m^{-1}$ and a is the particle radius in micrometers. This distribution is most uncertain below about 0.1 μm, a region important for non-gas-phase reactions, since much of the aerosol surface area might reside on the smallest particles. The distribution uncertainty does not significantly add to uncertainty in the ultraviolet and visible scattering properties of the exhaust, since most of the scattering is done by 0.5- to 5-μm particles. The altitude-dependent value for α is found by using a particle density ρ of 2.3 $g \cdot cm^{-3}$ and writing

$$m(z) = \frac{4\pi}{3}\rho \int_0^\infty N(a, z)a^3 \, da \tag{5}$$

where $m(z)$ is the alumina mass deposition as a function of altitude. In the results that follow, the concentration is shown for particles between 0.1 and 10 μm, where 91% of the exhaust alumina mass resides according to Eq. (4). It is possible that the number of particles smaller than 0.1 μm significantly exceeds the number larger than 0.1 μm; this would not affect our conclusions regarding the scattering of ultraviolet light, however.

Initial Conditions and Model Scenarios

Model initial conditions consist of the ambient stratospheric composition and the initial plume composition and dimension. The former is adopted from Shimazaki[12] for zero solar zenith angle. The latter is based on Zittel,[4] who predicts the Titan IV plume composition as a function of vehicle altitude. Zittel[4] and Dension et al.[5] are in substantial agreement on the relative amount of active chlorine and the lack of significant amounts of nitrogen oxides and molecular hydrogen in the post-afterburning plume. We emphasize that the initial conditions for our cold-plume model are unproved predictions from hot-plume models that include afterburning. Different assumptions regarding initial plume composition (i.e., hot-plume predictions) will result in different local ozone loss. The altitude dependence of the plume composition reflects increasing HCl afterburning and increasing vehicle velocity with altitude. Other plume constituents are either chemically unimportant over these timescales (e.g., H_2O and CO_2) or are present in negligibly small amounts (e.g., nitrogen compounds). The initial plume is assumed to be 1 km in diameter and homogeneous. The vehicle altitude as a function of distance downrange is from a 1993 Titan IV launch. The exact model zero time is not identical for each altitude and is not well defined in any case. The model can be considered to start at the time the plume has stabilized in altitude, about 6–12 min after vehicle passage and about 15 min after launch. All times are given as after launch with the understanding that model time differs from actual time by about 15 min. Table 2 shows the initial plume composition as a function of altitude for Cl, Cl_2, HCl, and aerosol particles. The other model species concentrations are assumed to be 10^8 cm^{-3}, a numerically convenient and arbitrary value meant to reflect the absence of that constituent in the SRM plume.

Since plume morphology is determined by the interplay between the seasonally variable stratospheric winds and the launch trajectory azimuth, the plume will behave differently for various launch trajectories at different times of the year. Stratospheric winds are fairly predictable and blow from the west (u_i positive) in northern-hemisphere winter and from the east (u_i negative) in summer; velocity generally increases with altitude. Thus, for example, after an eastward launch during summer the plume will tend to compress back on itself for a time and then stretch zonally to the west; during winter the same plume will quickly stretch out to the east. The three

Table 2 Titan IV plume initial conditions[a]

Constituent	Number density, cm^{-3}		
	15 km	30 km	40 km
HCl	2.4×10^{13}	3.9×10^{12}	2.7×10^{12}
Cl	7.1×10^{9}	9.2×10^{10}	4.6×10^{12}
Cl_2	3.6×10^{12}	4.6×10^{12}	3.1×10^{12}
Al_2O_3[b]	1760	1280	960

[a]Initial plume radius, 500 m. [b]0.1 $\mu m < a < 10$ μm.

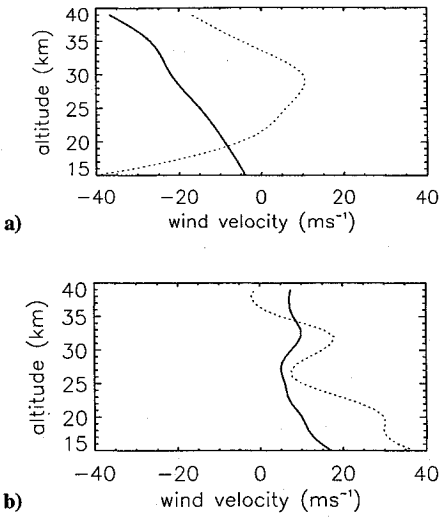

Fig. 1 Model stratospheric wind velocity for a) July and b) January. The solid and dotted lines are for zonal and meridional winds, respectively. The meridional velocity is multiplied by a factor 10 for clarity.

scenarios investigated present a range of wind and trajectory combinations: 1) an eastward launch during July, 2) a westward launch during January, and 3) a southward launch during January. An east launch or south launch can be taken to mean the Eastern Test Range or Western Test Range, respectively. Figure 1 shows the zonal and meridional winds for July and January, derived from the profiles of mean wind velocity and direction variance in the NASA/AF Range Reference Atmosphere.[21] Whereas the zonal wind velocity typically exceeds the zonal variance by a factor of at least 4, the meridional wind typically is of the same magnitude as meridional variance. Consequently, the exact shape and location of the plume will depend on the wind conditions that obtain during a specific launch, and the modeled plume evolution must be considered in a qualitative sense only, especially in the meridional direction.

Model Predictions

The model predictions are composed of two sets. First, number densities for important species are presented as a function of radius from plume center, $n(r)$, for different altitudes (20, 30, and 40 km) and times (1, 4, and 8 h after launch). These results are independent of stratospheric wind conditions. Second, maps of total stratospheric column loss are presented for 1 and 4 h after launch. A word here about nomenclature: we use "defect" for a region where the number density of a particular species has decreased, and "enhancement" for a region where it has increased.

Radial Distributions

Figures 2a–2i show the evolution of $n(r)$ for O, O_3, Cl, Cl_2, ClO, Cl_2O_2, CH_4, HCl, and Al_2O_3 at 20-km altitude. During the first hour very steep gradients sharply delineate the plume from the ambient stratosphere. This is true for all species. The atomic- and molecular-chlorine enhancements are about 4 and 8 km in diameter, respectively. The latter is larger because it diffuses away from the plume center before photolyzing into Cl, which reacts quickly with O_3 and CH_4. The ozone and methane defects are about 4 km in diameter. The enhancements of HCl, ClO, and Cl_2O_2 are somewhat larger, 6–8 km in diameter. The Cl_2O_2 enhancement has a defect at its center as a result of the fast reaction with Cl. The defects are smaller than the enhancements because in the former a reacting species is diffusing into a hole and disappearing. The enhancements, products of the ozone loss, diffuse away from the reaction site. After 1 h the aerosol scattering plume, defined[22] (arbitrarily) as the part of the plume where the Al_2O_3 number density exceeds 10 times the ambient number of particles greater than 0.1 μm is about 12 km in diameter.

In the subsequent 3 h the most dramatic features of the plume disappear. Cl and Cl_2 have declined to concentrations below ambient ozone and methane. The deep ozone and methane defects have filled

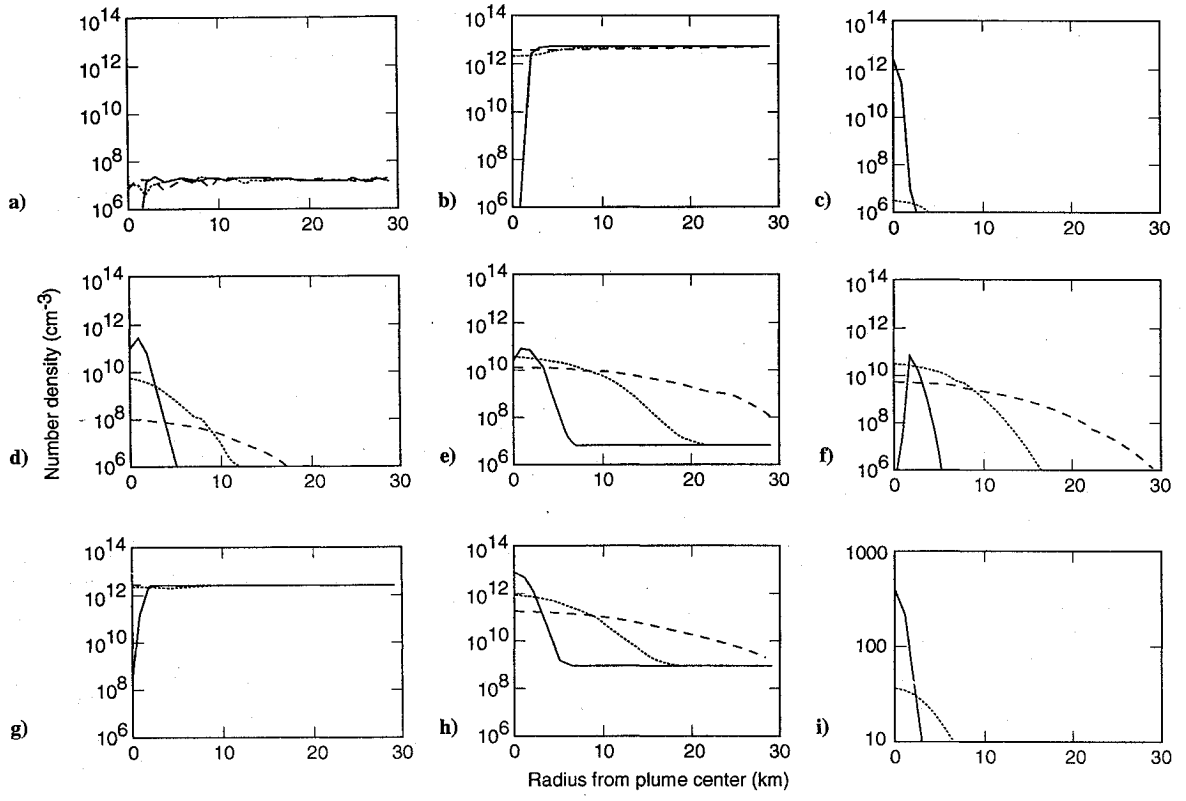

Fig. 2 Number density as a function of radius from plume center for a) O, b) O_3, c) Cl, d) Cl_2, e) ClO, f) Cl_2O_2, g) CH_4, h) HCl, and i) Al_2O_3. Altitude is 20 km. The solid, dotted, and dashed lines are for 1, 4, and 8 h after launch, respectively.

in. However, even though the most intense part of the defects has disappeared, the loss region continues to expand. Elevated chlorine levels continue to cause ozone loss, and the horizontally integrated amount of ozone at this altitude continues to decrease. Ambient ozone production is slow at 20 km, with a time constant of months, so that the ozone defect can be ameliorated only though diffusion of ozone-rich ambient air; this is true for methane as well. Meanwhile the HCl, ClO, and Cl_2O_2 enhancements continue to expand so that the reaction plumes in these cases have become about 20–25 km in diameter. After 4 h the aerosol plume is about 12 km in diameter. After 8 h the deep defects are gone; the maximum ozone loss is 12%. Large HCl, ClO, and Cl_2O_2 enhancements remain and are now about 40 km in diameter; the aerosol plume has disappeared.

Figures 3a–3i show the evolution of the plume at 30-km altitude. The evolution during the first hour is similar to the situation at 20 km. The main difference is that the production of Cl_2O_2 is less than at 20 km; the maximum concentration is about an order of magnitude less than at the lower altitude. After 4 h, the most dramatic features of the plume, the deep defects, have not yet disappeared and are about 14 km in diameter. The chlorine enhancements remain within an order of magnitude of the ambient ozone level. After 8 h the ozone and methane defects are about 15 km in radius and are just beginning to fill. The aerosol plume evolution closely resembles the situation at 20 km, since the alumina load is similar at all altitudes.

Figures 4a–4i show the evolution of the plume at 40-km altitude. Once again the evolution during the first hour resembles the 20- and 30-km cases. After 4 h the ozone and methane defects are about 26 km in radius. Even after 8 h the deep defects continue to expand and have only barely started to disappear. Cl_2O_2 production is negligible here, so that the amount of Cl_2 is small and the amount of ClO (relative to ozone) is large compared to the plume at lower altitudes. In contrast to 20 and 30 km, significant amounts of Cl remain after 8 h, suggesting the ozone loss will continue and the ozone defect will expand further.

Despite different initial plume composition assumptions and diffusion parameters, we wish to compare our results against previous work. The model of Denison et al. is similar to this work in that they adopted the same SRM afterburning scenario in a vehicle without liquid motors; their model SRM was about $\frac{1}{10}$ the mass of the Titan IV motors, however. They found transient ozone loss lasting no more than a few minutes over areas of a fraction of a square kilometer. Karol et al. modeled a Space Shuttle launch with almost all exhaust chlorine as Cl_2 and found transient ozone loss lasting several hours over areas of tens of square kilometers, in substantial agreement with our results. Kruger also modeled Space Shuttle exhaust with 50% free chlorine and also found transient ozone loss lasting several hours over several square kilometers. The ozone loss predicted by Kruger is less severe than predicted here or by Karol et al. and may be the result of Kruger's including substantial amounts of H_2 in the shuttle exhaust ($H_2 + Cl \rightarrow HCl + H$). This may not be realistic, however, since H_2 may be expected to be consumed during afterburning, even for the Space Shuttle liquid motors. Our results are in basic agreement with Karol et al. and to a lesser extent, Kruger. It is difficult to ascribe the short plume lifetime reported by Denison et al. simply to motor size. We suspect that differences in model diffusion rates are responsible; in Denison et al., with larger diffusion coefficient, the plume disperses before Cl_2 has time to photodissociate. The differences between our model and previous work can largely be attributed to differences in initial conditions and diffusion parametrizations rather than the level of sophistication of the chemistry schemes. Still, these disparate results point to the need for a better understanding of the composition of post-afterburning solid-and liquid-motor exhaust.

Our purpose has been to show that the massive amounts of chlorine from the SRMs and the relative speed of the oxygen–chlorine reactions make it possible to model the SRM stratospheric plume with a limited chemistry scheme. This in turn allows us concentrate on plume dynamics and two-dimensional evolution of the defect in the total ozone column abundance.

We would like to make a few final points concerning the model. The results after 8 h are suspect for a variety of reasons. First, vertical diffusion will be a factor by this time, especially after the plume has been sheared to the point that plume centers at different altitudes are separated by a distance exceeding the plume radius. Second, 8 h

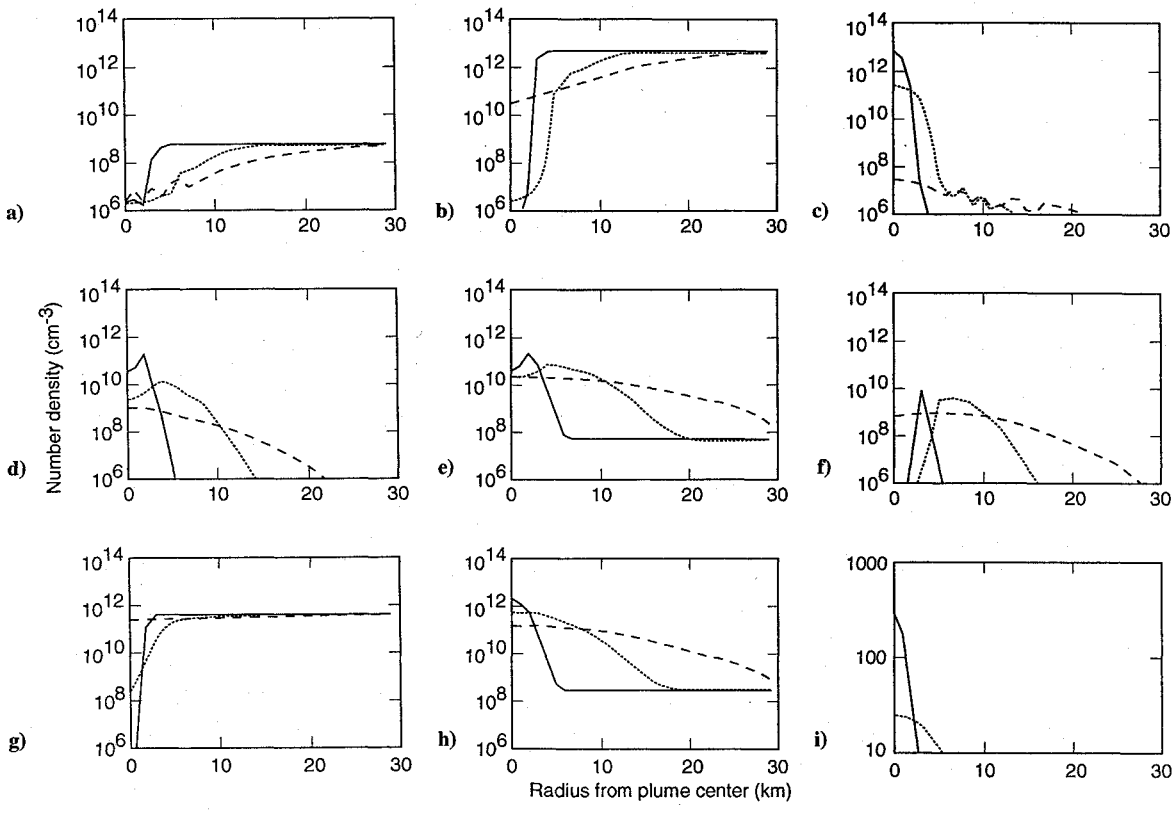

Fig. 3 Same as Fig. 2, except altitude is 30 km.

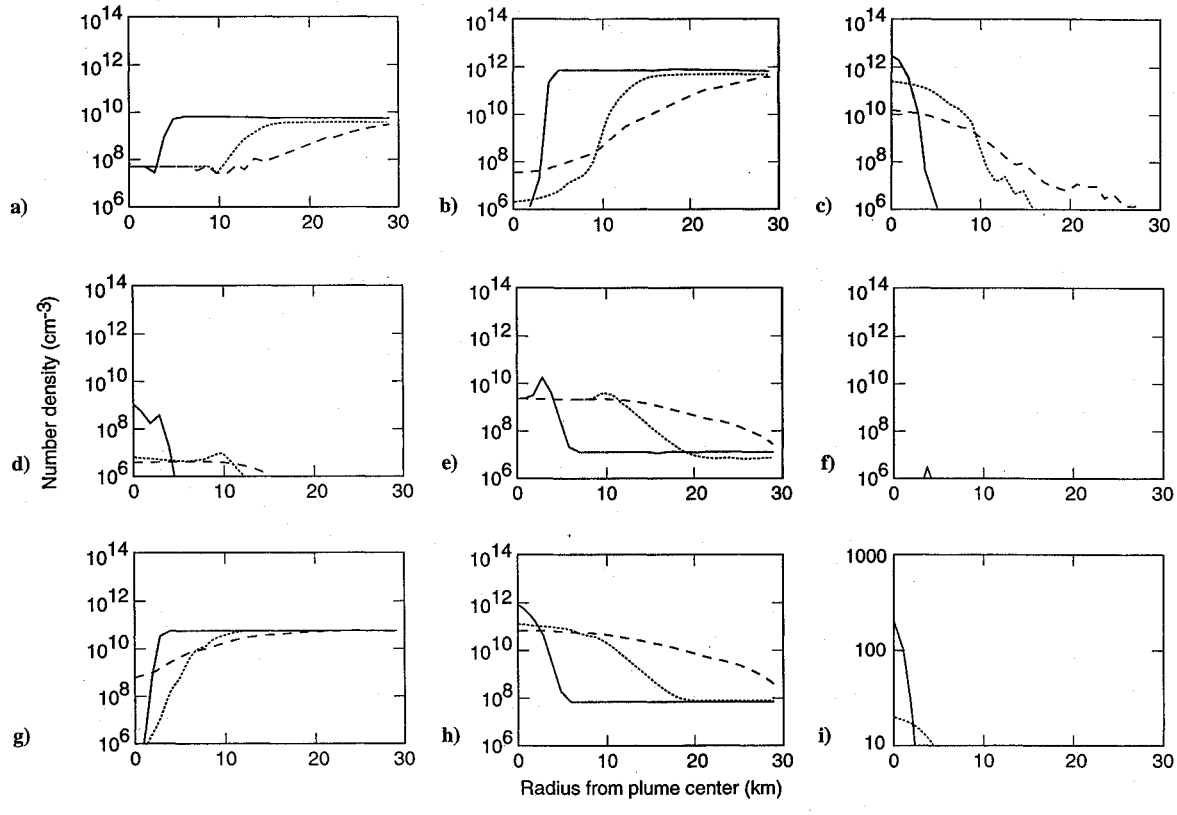

Fig. 4 Same as Fig. 2, except altitude is 40 km.

roughly corresponds to the end of daylight after a daytime launch. (The exact time of launch is not critical to the results, as noted above.) Once the sun sets, the chemistry changes; the main difference is that the photolysis of ClO and Cl_2 ends. The plume continues to disperse during the night; by this time the diffusion coefficient is quite large, several thousand $m^2 \cdot s^{-1}$. During the night, the enhancements will decline to a few percent of the 8-h values. There will be a second, much less intense period of ozone loss after sunrise over a large area, an echo of the previous day's launch. Vertical shear will eventually fragment the plume, and it will lose its identity as a coherent structure. The time to replace the lost ozone is long—weeks to months, depending on altitude. The defect therefore remains, but will disperse over a such a wide area as to be unobservable and of no local environmental significance after at most a few days.

Total Ozone Loss

The column ozone abundance Ω is the ozone number density integrated from the surface to the top of the atmosphere. Remote-sensing techniques that make use of ozone absorption of solar light measure the column abundance, so maps of Ω are needed to predict how the plume would appear to absorption instruments at various times after launch within the context of spatial resolution and sensitivity. Figures 5–7 show contour maps of the percentage decrease of Ω for the three cases of time of year and launch azimuth. The origin of the coordinate system in each figure is arbitrary, and the scale varies from figure to figure (the results of plotting plume structures with different scales on a constant-size figure). The caption for each figure gives the location of the launch site in the coordinate system specific to that figure.

Figures 5a and 5b show the percentage decrease in Ω for the eastward July case 1 and 4 h after launch, respectively. Here, the wind blows the plume westward back over the launch site and across the Florida peninsula. The plume passes nearly directly over the launch site about $\frac{1}{2}$ h after launch. After 1 h the main part of the Ω defect (arbitrarily defined as loss greater than 8%) is an elongated region about 100 km^2 in area. The maximum loss of 28% is located about 82 km west and 5 km south of the launch site. In a very large region of about 700 km^2, the loss exceeds 2%. After 4 h the plume has been elongated in the zonal direction by the strong westward winds. The main part of the Ω defect is an oval region about 2300 km^2 in area. The peak loss has declined to 17% and is now about 320 km west and about 20 km south of the launch site.

Figures 6a and 6b show the percentage decrease in Ω for the eastward January case 1 and 4 h after launch, respectively. Here the plume is blown eastward out over the Atlantic Ocean by the stratospheric winds. After 1 h the main part of the Ω defect includes two regions separated by about 20 km with a total area roughly equal to that in Fig. 5a. The peak loss of 29%, also similar to Fig. 5a, is about 64 km east of the launch site. After 4 h the plume has expanded, but is not as elongated as for the July case previously considered, since January winds are more nearly constant with altitude. The main part of the Ω loss covers about 1300 km^2, considerably less than the July case, and the maximum loss is 23%, somewhat greater than the July case.

Figures 7a and 7b show the percentage decrease in Ω for the southward January case 1 and 4 h after launch, respectively. In this case

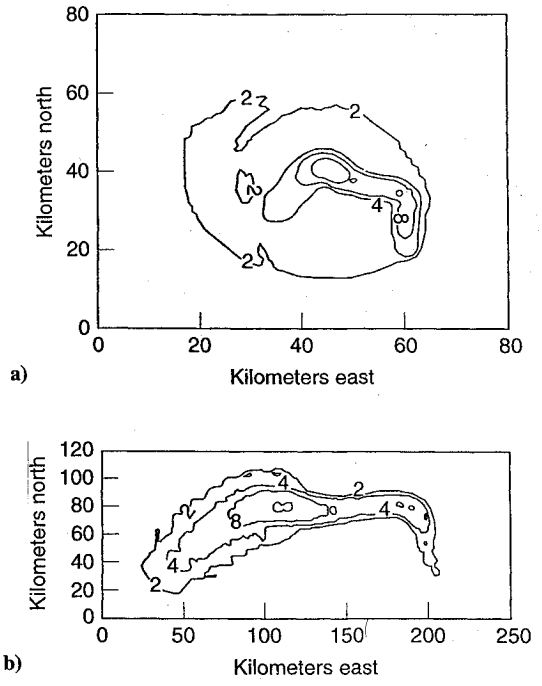

Fig. 5 Map of the percentage decrease of total column abundance of ozone Ω: a) 1 h and b) 4 h after launch. The launch direction is eastward, and the stratospheric wind model is for July at Cape Canaveral. Zero loss corresponds to 350 Dobson units. The launch site is located at a) 127 km east and 45 km north and b) 432 km east and 98 km north.

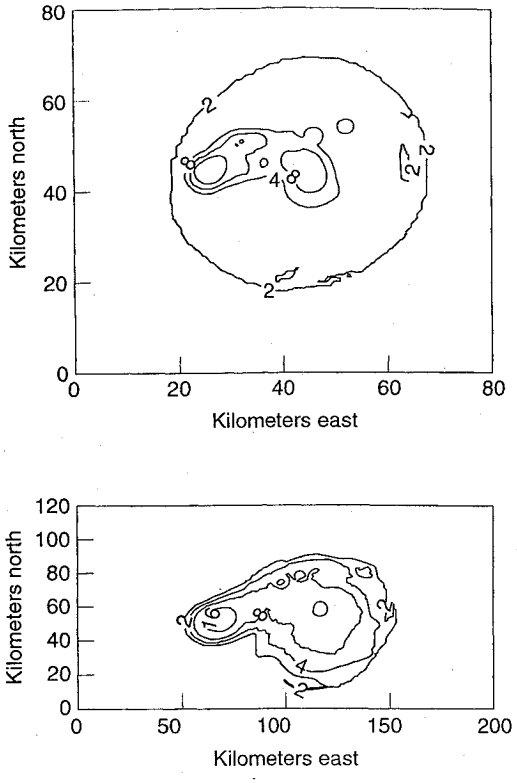

Fig. 6 Map of the percentage decrease of total column abundance of ozone Ω: a) 1 h and b) 4 h after launch. The launch direction is eastward, and the stratospheric wind model is for January at Cape Canaveral. Zero loss corresponds to 350 Dobson units. The launch site is located at a) −19 km east and 40 km north and b) −211 km east and 34 km north.

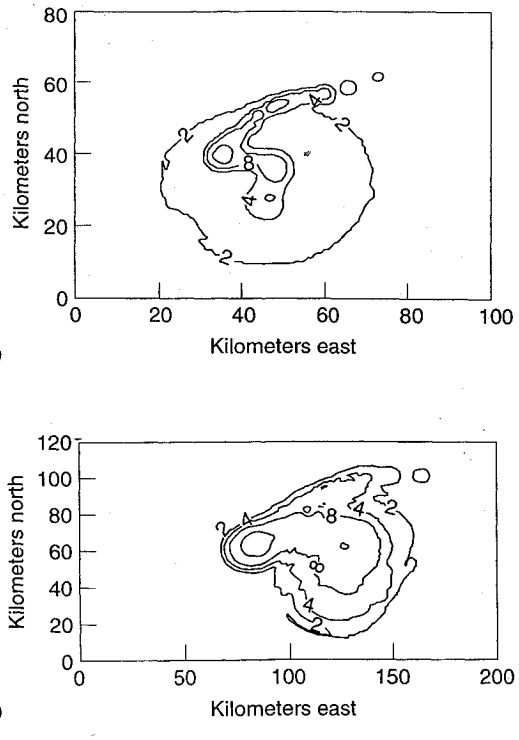

Fig. 7 Map of the percentage decrease of total column abundance of ozone Ω: a) 1 h and b) 4 h after launch. The launch direction is southward, and the stratospheric wind model is for January at Cape Canaveral, which can be considered an adequate model for Western Test Range January winds. Zero ozone loss corresponds to 350 Dobson units. The launch site is located at a) 10 km east and 57 km north and b) −38 km east and 93 km north.

the launch direction and winds are nearly orthogonal. The main part of the Ω loss here is more irregular in shape than the cases above; the irregularity is driven mainly by vertical shear in the wind component normal to the launch direction. Here the trajectory normal wind is zonal and so has larger vertical shear than the meridional wind that is normal to the trajectory in the cases above. The maximum loss is only 23%, less than the other two cases. By 4 h after launch the plume looks remarkably similar to the eastward January case above. This shows that wind conditions completely dominate plume morphology after a few hours.

In each of the three cases the maximum ozone column loss significantly exceeds the value of 10% previously mentioned as the maximum loss in the plume.[23] In this model the total number of ozone molecules lost is not dependent on trajectory or winds. The maximum and area of significant ozone column loss are dependent on wind and trajectory by about a factor of 2. Thus some launches at some times of the year would be easier to observe than others, depending on the instrument. Results were not presented for 8 h after launch, since the plume has been very highly sheared by this time, and the regions involved become very large, up to a thousand kilometers zonally. By 8 h, adjacent plume layers have been sheared by distances comparable to the radius of the ozone defect so that the column loss is increasingly dominated by the loss in at most a few layers and the decrease in Ω is less than a few percent everywhere.

Ultraviolet Flux

A complete calculation of the radiation intensity in and around the plume is beyond the scope of this paper. A fully three-dimensional, multiple-scattering radiative transfer model is required. It is desirable, however, to include a simple model of the ultraviolet intensity in the plume, for two reasons. First, the environmental concern over ozone loss centers on the potential for increased levels of harmful solar ultraviolet flux on the ground. A simple model can provide a preliminary understanding of the environmental implications of SRM ozone depletion. Second, ultraviolet remote sensing that depends on the absorption and scattering properties of the stratosphere is frequently used to measure stratospheric ozone, from the ground and space. We are interested, therefore, in how the complete plume composition influences the ultraviolet spectrum of sunlight that has passed through the plume.

As we mentioned above, the most important changes in the ultraviolet radiance in the plume are the loss of ozone absorption and the addition of aerosol scattering, which increase and decrease the ultraviolet flux for locations on the ground where the plume is between the observer and the sun. Second-order effects include ultraviolet absorption by gases that are present in small amounts in the ambient stratosphere but in large amounts in the plume. As we have shown (Figs. 2–4), a fraction of the ambient ozone in the plume is replaced by a mixture of Cl_2, ClO, and Cl_2O_2, the relative amounts varying with time, position with respect to the plume centerline, and altitude. These plume constituents possess[24] absorption cross sections comparable to, or exceeding, the ozone cross section at wavelengths exceeding about 290 nm.

The intensity of ultraviolet light transmitted through the stratosphere at the top of the troposphere, $I_t(\lambda)$, is given as

$$I_t(\lambda) = I_s(\lambda)\exp[-\tau_a(\lambda) - \tau_s(\lambda)] \tag{6}$$

The ultraviolet flux on the ground is determined by I_t and the scattering properties of the troposphere. Now because of tropospheric scattering, the spectrum of ultraviolet light reacting a ground observer is influenced by an extended region of the stratosphere centered on the observer–sun line. At wavelengths near 300 nm, the horizontal extent of the sampled region roughly equals the scale height of the lower troposphere, about 8 km. Therefore, for the purpose of calculating optical properties of the plume with respect to the ground, column abundances should be an average value in an 8-km-diam column centered on the observer–sun line. Assuming fixed tropospheric properties, changes in I_t can be understood to relate linearly to changes in the ultraviolet flux on the ground, our main interest. Model predictions of the total column abundances of O_3, Cl_2, ClO, and Cl_2O_2 determine the stratospheric absorption optical depth τ_a, which is given by

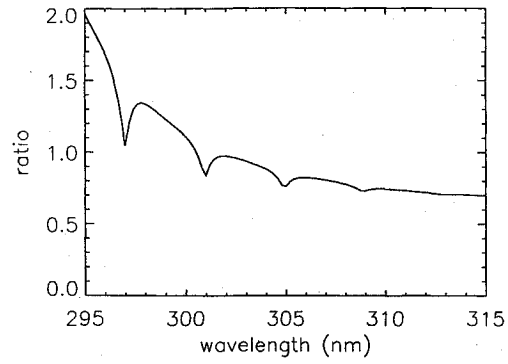

Fig. 8 Ultraviolet flux on the ground beneath the location of maximum ozone loss (from Fig. 5a) divided by the undisturbed ultraviolet flux as a function of wavelength in the UV-B waveband for the overhead sun.

$$\tau_a(\lambda) = \sum \Gamma_i \sigma_i(\lambda) \tag{7}$$

where Γ_i is averaged in a column 8 km in diameter centered on the maximum ozone loss; and the sum is taken for O_3, Cl_2, ClO, and Cl_2O_2. From the case of Fig. 5a, model Γ_i predictions for these species are 7.5×10^{18} (20% loss), 5.0×10^{16}, 1.0×10^{17}, and 5.6×10^{16} cm^{-2}, respectively. The stratospheric aerosol scattering optical depth is given by

$$\tau_s = \int_{15\text{ km}}^{40\text{ km}} \int_{0.1\ \mu\text{m}}^{10\ \mu\text{m}} \pi Q(a) N(z, a) a^2 \, da \, dz \tag{8}$$

where $Q(a)$ is the alumina scattering efficiency, calculated using Mie theory assuming nonabsorbing spherical particles with index of refraction[25] of 1.6 at a wavelength of 300 nm. The value of Q is only weakly dependent on wavelength and is taken as constant. $N(z, a)$ is from the model prediction, averaged in a column 8 km in diameter centered on the maximum ozone loss. The model predicts that τ_s equals 0.42. We note that micrometer-size alumina particles will forward-scatter solar ultraviolet, meaning that some light will reach the ground after being scattered in the plume, reducing the effective magnitude of τ_s. Accordingly, the value 0.42 should be taken as an upper limit.

From Eqs. (6–8), Fig. 8 shows the ratio of the perturbed noon ultraviolet flux to the undisturbed noon flux on the ground beneath the maximum ozone loss of 28% one hour after launch (from the case in Fig. 5a). The waveband in Fig. 8 includes most of the spectral region known as UV-B, frequently used by remote-sensing instruments and the most important solar ultraviolet region from a biological perspective.[26] The outstanding features of the UV-B spectrum under the plume are a large increase at wavelengths less than about 303 nm from ozone loss and a decrease at longer wavelengths caused by alumina scattering (the latter effect being the plume shadow). The features in the spectrum near 297, 301, and 305 nm are caused by ClO absorption. This simple calculation shows that because of scattering by plume aerosols and absorption by chlorine oxides, perturbations in the ultraviolet flux on the ground beneath ozone-poor SRM plumes cannot be assumed to increase at all wavelengths. With the caveat that the spectrum at the plume edges may be quite different from Fig. 8, the roughly 10-km zonal dimension of the deepest ozone loss and lower stratospheric winds of about 20 m · s^{-1} suggest that the UV-B disturbance will last about 500 s on the ground as the plume passes overhead. At later times the ultraviolet disturbance will be less intense but last longer. Although Fig. 8 is suggestive of a certain level of UV-B dose increase for regions under the plume, we conclude that a more realistic radiative model is required to conclusively quantify the environmental effects of the ultraviolet flux changes underneath the plume, viz., whether the total UV-B dose increases or decreases.

Remote measurement of plume ozone loss using ultraviolet absorption techniques is made difficult by the small scale of the plume

(tens of kilometers), chlorine oxide absorption, and alumina scattering, as demonstrated by Fig. 8. The total ozone mapping spectrometer (TOMS) possesses the best horizontal resolution of space-based Ω measurements available. The TOMS field of view (FOV) covers about 1600 km^2; its measurement standard deviation is about 3%. (Other space-based ozone instruments have much larger FOVs and could not possibly see SRM ozone loss.) From Fig. 5b, for example, the plume area with ozone loss exceeding 8% is just larger than the area of the TOMS FOV, and one might expect to detect the plume ozone defect 4 h after launch were the FOV located exactly over the maximum ozone loss. McPeters et al.[27] examined Nimbus 7 TOMS measurements taken at various times after eight Space Shuttle launches and concluded that TOMS data do not support the existence of severe localized ozone loss following SRM use. But the data they examined consisted of Ω maps returned by the TOMS data analysis algorithm, which does not allow for absorption by plume gases or scattering by plume aerosols. Given a marginal ability to resolve the plume and the complex radiative plume environment, we conclude that TOMS solar backscatter data must be examined more carefully before being used to confirm or deny the existence of local SRM ozone loss of the magnitude predicted here. An imaging spectrograph recording the complete midultraviolet spectrum with horizontal resolution of a few kilometers is required to confidently measure ozone loss in the plume using space-based solar backscatter. Such an instrument should also have a polarametric capability to help distinguish Rayleigh scattering from plume aerosol scattering.

Summary

Large SRMs significantly perturb the stratosphere locally during the first day after launch. If afterburning in the hot exhaust plume includes the liberation of significant amounts of Cl or Cl_2 from HCl, the main characteristic of this perturbation is ozone loss brought about by the rapid reaction of chlorine and ozone. Ozone-depleted regions form as chlorine-rich exhaust mixes with the surrounding stratosphere. We present a model of this process and show how the ozone defect evolves during the first day after the launch of a Titan IV vehicle. A deep ozone defect appears promptly, in which ozone concentrations decrease by several orders of magnitude. In the lower stratosphere the deep ozone defect expands from about 2–10 km in radius during the first 4 h after launch. In the upper stratosphere the defect reaches 40-km radius and lasts into the first night after launch. Throughout the stratosphere, large regions (up to 40 km in radius) form in which chlorine oxide species are elevated above the background by several orders of magnitude. The disturbed regions at different altitudes advect according to the vertical profile of stratospheric winds, and the resulting hole in the total column ozone abundance elongates in the zonal direction. One hour after launch, the maximum loss in total ozone is about 30%, declining to about 20% after 4 h. The plume expands and is sheared by stratospheric winds, eventually disappearing as SRM chlorine reacts with ambient methane to form HCl, the main chlorine sink in the stratosphere, and the plume mixes with ambient ozone-rich air.

Our model makes a number of assumptions regarding the initial composition of the cold plume that influence the result; different choices would produce different results. If afterburning does not produce the significant amounts of active chlorine assumed here, there will be much smaller, perhaps insignificant, ozone loss. By not including hydrogen and nitrogen species and aerosols in the kinetics scheme, we ignore several potential increases in ozone loss (from catalytic cycles and aerosol surface reactions) and potential decreases in ozone loss (from chlorine and chlorine oxide sinks). The net result of including all of these in a comprehensive model is uncertain, but they are not likely to be a factor during the first few hours after launch. The present model must be considered robust, however, in that significant active chlorine production necessarily leads to local ozone loss.

Whereas the stratospheric mass loading of the Titan IV is of the same order as the loading of other vehicles such as the Space Shuttle and Ariane V, this work may not be applicable to those vehicles because of uncertainties in the initial composition of liquid-motor cold plumes. In these cases, the severity and area of the local ozone loss will depend not only on the amount of free chlorine production in the SRMs, but on the production of important liquid-motor exhaust species not present in SRM exhaust, H_2 and NO for example. The former would tend to decrease ozone loss by consuming Cl, and the latter would consume ozone directly. Again, the net effect in a comprehensive model is uncertain.

The radiative effects of changes in stratospheric composition on the scale of a Titan IV plume are difficult to predict, but a simple model shows that the ultraviolet flux on the ground under the plume is predicted to increase substantially at wavelengths less than about 303 nm. At longer wavelengths the change in flux is determined by the competing effects of decreased ozone absorption and alumina scattering, and the ultraviolet flux may decrease in this spectral region. The net UV-B dose rate may in fact decrease beneath the plume, despite ozone loss. Chlorine oxide absorption plays a smaller role that nevertheless could, along with the alumina scattering, interfere with ultraviolet absorption techniques to measure ozone loss in the expanding plume. Present instrumentation such as TOMS does not possess the spatial resolution or spectral coverage required to detect SRM ozone loss; higher spatial resolution and more complete spectral coverage are required.

Acknowledgments

This work was supported by the Aerospace Sponsored Research Program and the U.S. Air Force Space Missile Systems Center Contract No. F04-701-91-C-0008. The author would like to thank D. L. Anderson, B. B. Brady, V. I. Lang, L. R. Martin, and P. F. Zittel for helpful discussions.

References

[1]Prather, M. J., Garcia, M., Douglass, A. R., Jackman, C. H., Ko, M. W., and Sze, N. D., "The Space Shuttle's Impact on the Stratosphere," *Journal of Geophysical Research*, Vol. 95, No. D11, 1990, pp. 18,583–18,590.

[2]Anon., "Atmospheric Effects of Chemical Rocket Propulsion," Rept. of AIAA Workshop, AIAA, Washington, DC, June 1991, p. 52.

[3]Ko, M., Sze, N., and Prather, M., "Better Protection of the Ozone Layer," *Nature*, Vol. 367, No. 6463, 1994, pp. 505–509.

[4]Zittel, P., "Computer Model Predictions of the Local Effects of Large Solid Rocket Motors on Stratospheric Ozone," Aerospace Corp., ATR 4092-92, Los Angeles, CA, 1994.

[5]Denison, M., Lamb, J., Bjorndahl, W. D., Young, E. Y., and Lohn, P., "Solid Rocket Exhaust in the Stratosphere," *Journal of Spacecraft and Rockets*, Vol. 31, No. 3, 1994, pp. 435–442.

[6]Pergament, H., Gomberg, R., and Poppoff, I., "NO_x Deposition in the Stratosphere from the Space Shuttle Rocket Motors," NASA TM JSC-11633, 1977, Appendix G.

[7]Karol, I., Ozolin, Y., and Rozonov, E., "Effect of Space Launches on Ozone," *Annales Geophysicae*, Vol. 10, No. 10, 1992, pp. 810–814.

[8]Kruger, B. C., "Ozone Depletion in the Plume of a Solid Rocket Motor," *Annales Geophysicae*, Vol. 12, No. 5, 1994, pp. 409–416.

[9]Stott, P., and Harwood, R., "An Implicit Time Stepping Scheme for Chemical Species in a Global Atmospheric Circulation Model," *Annales Geophysicae*, Vol. 11, No. 5, 1993, pp. 377–388.

[10]DeMore, W., Sander, S., Goldin, D., Molina, M., Hampson, R., Kurylo, M., Howard, C., and Ravishankara, A., "Chemical Kinetics and Photochemical Data for Use in Stratospheric Modeling," NASA JPL Publication 90-1, 1990.

[11]Anon., "Predicted Rocket and Shuttle Effects on Stratospheric Ozone," World Meteorological Organization, Rept. 25, Geneva, Switzerland, 1991, Chap. 10.

[12]Shimazaki, T., *Minor Constituents in the Middle Atmosphere*, Terra Scientific Press, Tokyo, 1985, p. 455.

[13]Pasquill, F., *Atmospheric Diffusion*, Wiley, New York, 1974, p. 426.

[14]Hocking, W., "Measurements of Turbulence and Its Evolution During MAP," *COSPAR Symposium 6*, 1989, pp. 104–122.

[15]Danielson, E., and Louis, J., "Transport in the Stratosphere," *The Upper Atmosphere and Magnetosphere*, National Academy of Sciences, Washington, DC, 1977, pp. 141–155.

[16]Danilin, M., Kruger, B., and Ebel, A., "Short-Term Atmospheric Effects of High-Altitude Aircraft Emissions," *Annales Geophysicae*, Vol. 10, Nos. 11, 12, 1992, pp. 904–911.

[17]Turco, R., Whitten, R., and Toon, O., "Stratospheric Aerosols: Observation and Theory," *Reviews of Geophysics*, Vol. 20, No. 2, 1982, pp. 233–279.

[18]Hamill, P., and Toon, O., "Polar Stratospheric Clouds and the Ozone Hole," *Physics Today*, Vol. 44, No. 1, 1991, pp. 34–42.

[19]Dave, J., "Effect of Aerosols on the Estimation of Total Ozone in the Atmospheric Column from the Measurements of Its Ultraviolet Radiation," *Journal of Atmospheric Science*, Vol. 35, No. 5, 1978, pp. 899–911.

[20]Cofer, W. R., Bendura, R. J., Sebacher, D. I., Pellet, G. L., Gregory, G. L., and Maddrea, G. L., "Airborne Measurements of Space Shuttle Exhaust Constituents," *AIAA Journal*, Vol. 23, No. 2, 1985, pp. 283–294.

[21]Anon., "Range Reference Atmosphere," Range Commanders Council, Document 361–383, White Sands, NM, 1983.

[22]Toon, O. B., and Farlow, N. H., "Particles Above the Tropopause: Measurements and Models of Stratospheric Aerosols, Meteoric Debris, Nacreous Clouds, and Noctilucient Clouds," *Annual Review of Earth and Planetary Science*, Vol. 9, No. 1, 1981, pp. 19–58.

[23]Jackman, C., "The Impact of Emissions from Space Transport Systems on the State of the Atmosphere," *Proceedings of an International Scientific Colloquium on Ozone Depletion*, Inst. für Physik der Atmosphäre, Cologne, Germany, 1994, pp. 366–371.

[24]Burkholder, J., Orlando, J., and Howard, C., "UV Absorption Cross Sections of Cl_2O_2 Between 210 and 410 nm," *Journal of Physical Chemistry*, Vol. 94, No. 2, 1990, pp. 687–691.

[25]Parry, D. L., and Brewster, M. Q., "Optical Constants of Al_2O_3 Smoke in Propellant Flames," *Journal of Thermophysics and Heat Transfer*, Vol. 5, No. 1, 1991, pp. 142–149.

[26]Anon., "Cause and Effects of Stratospheric Ozone Reduction," Rept., Environmental Studies Board of the National Research Council, National Academy Press, Washington, DC, 1982.

[27]McPeters, R., Prather, M., and Doiron, S., "Reply to Aftergood," *Journal of Geophysical Research*, Vol. 96, No. D9, 1991, pp. 17,379–17,381.

I. D. Boyd
Associate Editor